

# Monolithic Hyper ROM FE<sup>2</sup> Method with Clustered Training at Finite Deformations

Nils Lange, Geraf Hütter, Bjoern Kiefer

June 6, 2023

## Abstract

The usage of numerical homogenization to obtain structure-property relations using the finite element method at both the micro and macro scale has gained much interest in the research community. However the computational cost of this so called FE<sup>2</sup> method is so high, that algorithmic modifications and reduction methods are essential. Currently the authors proposed a monolithic algorithm. Now this algorithm is combined with ROM and ECM hyper integration, applied at finite deformations and complemented by a clustered training strategy, which lowers the training effort and the number of necessary ROM modes immensely. An implementation in terms of an extension for the already established MonolithFE<sup>2</sup> code is provided. Numerical examples show the efficiency and accuracy of the monolithic hyper ROM FE<sup>2</sup> method and the advantages of the clustered training strategy. The applied methods are modularly combinable as aimed in finite element approaches.

## 1. Introduction

Nearly all materials relevant for engineering show characteristic inhomogeneities at a certain length scale. Aiming to describe the materials behavior in an adequate accuracy, it usually is sufficient to use homogenized material laws working with a strain definition as observable state variable and a set of internal state variables with evolution laws for the associated forces, aiming to describe all macroscopically observed effects, while ensuring thermodynamic consistency. For certain very complex microstructures e. g. composites or foams, homogenized materials may be hard to find, but usually the behavior of the individual components is known. Resolving the microstructure fully in a structural model is usually unfavorable, since firstly the microstructure is often not known everywhere in the sense of actual data e.g. from CT examinations and secondly the computational effort becomes tremendously high for large scale separations.

The necessity of solving these problems often leads to the common way of multiscale modeling using the assumption of a clear scale separation, which may be seen as a model reduction step. It is hypothesized that a representative volume element (RVE) can be found, including all essential microstructural defects and inclusions and showing statistically the same mechanical behavior as the actual microstructure, which describes the behavior of the point of a structure using the principle of local action.

The idea of examining the scale transition between a heterogeneous material and a structural level are of fundamental interest. This can be seen from the fact, that basic concepts already go back to the second half of the 19<sup>th</sup> century. From this time originates the Voigt bound, later the Reuss, Hill, Kröner etc. bounds were proposed, an overview can be found in [18]. An important fundamental consideration concerning the scale transition was the condition of macro homogeneity [17]. Later more distinct analytical homogenization approaches like the Mori-Tanaka method [34] were proposed. The computational resources in this time period were too restricted to even consider concurrent multiscale concepts. Due to the exponential growth of computer power according to Moores law, F. Feyel was able to present an implementation in the late 1990s [6], which linked a coarse and fine scale, whereby on both levels the finite element method (FEM) was used, for which he coined the term “FE<sup>2</sup> method”. This method developed out of an engineering research environment, whereas more mathematically oriented researches came to a similar approach which is call “FE-HMM”, cf. a comparison of the approaches and a nonlinear version of the FE-HMM in [4] and [5]. Other multiscale methods that leave behind the continuum assumption e.g. peridynamics that are also frequently used, are outside of the scope of this article. In view of the enormous amount of research activity in the field of multiscale modeling, overview articles like [23], [11], [41], [12], [32], [36], [7] are necessary to classify and compare the different concepts.

arXiv:2306.02687v1 [math.NA] 5 Jun 2023

Recently more and more research groups from completely different backgrounds pour into the scene, since its been observed, that the numerical multiscale concept using homogenization is not only suited for mechanical problems, but also for electro-magnetic, chemical, biological issues and their interrelationship. Regarding the placement of the approaches into Gartners hype cycle, Fish et. al. rank the current state into the phase of “Disillusionment” [7]. The expectations starting from the early innovation triggers rose to a hype of thinking “with these new simulation methods one can simulate *everything*”. Now a state of depression has arrived in the collective thinking, because it is realized, that the computational resources are often too restricted for even the smallest realistic problems. This comes from the fact that if using the finite element method on both levels, then behind every macroscopic integration point a very expensive microscopic FE model has to be computed. An incomplete list of the common endeavors to reduce the computational effort is:

1. Macroscopic elements with reduced integration
2. Approximation of the macro tangent e.g. Quasi-Newton algorithm
3. Massive parallelization in the macroscopic element loop
4. Usage of a monolithic (“true”) Newton scheme instead of a staggered one
5. Fast-Fourier Transformation (FFT) solver on the micro level
6. Description of the macroscopic material behavior via Neural Networks trained with micro FE simulations
7. Application of Reduced Order Modeling (ROM) together with hyper integration at the micro level

While the first 5 ideas represent only algorithmic variations of the original method, approaches 6 and 7 have an approximative character. Neural Networks are quite common in many recent applications. When the material response is nonlinear elastic, they are capable of describing a material very accurately and efficiently. When the material response is irreversible, much more complicated considerations must be taken into account. There are e.g. hybrid models [42],[20],[35],[31],[22], or so-called deep neural networks [28],[10] to ensure thermodynamic consistency. A review article classifying these methods can be found in [27], in which it is stressed that certain constraints must be present to ensure, that physically plausible and interpretable results will be obtained. These considerations however must be taken into account for every class of material and are hardly to be generalized. The idea 7, which was to the best knowledge of the authors first applied by Hernández et al. [16] in the nonlinear/irreversible multiscale context and picked up by various other authors e.g. [3],[40],[45], however directly ensures a physical material description especially under irreversible behavior, because it keeps the properties of the original FE<sup>2</sup> model without the need for special considerations, which is why this article only focuses on this approach. It is worth mentioning, that a similar method was also proposed for the FFT formulation, whereby in complete analogy a reduced set of Fourier Modes is constructed and a lower set of integration points is chosen [47]. Other sophisticated methods relying also on the reduced basis approach but moving further away from the FE<sup>2</sup> idea towards hybrid approaches e.g. the works of Fritzen et al. [9], [8], [43] and the usage of multiscale ROM methods outside the sole mechanical context e.g. in the analysis of heterogeneous poroelastic media [21], are outside of the scope of this research.

This article has mainly six goals. At first an efficient way of handling finite deformations in the context of the ROM FE<sup>2</sup> method is presented. Secondly the incorporation of the monolithic algorithm into the ROM method is shown. Thirdly the original proposal of the Empirical Cubature Method (ECM) by Hernández et al. is revisited and applied. Fourthly a clustered training strategy is introduced in order to reduce the training cost and fifthly an implementation for the commercial software Abaqus is shown. Finally numerical examples are provided, proving the computational efficiency and accuracy of the presented approaches.

## 2. Multiscale modeling

The main idea of multiscale modeling lies in the fact, that often specific distinct scales with a large contrast between their characteristic lengths exist, that influence each other, but whose local phenomena are to be modeled at the correct scale to get a meaningful effect description. Scales are e.g. the interaction between different galaxies, sun systems in a galaxy, planets in a sun system, movement and deformation of body’s on a planet, the deformation of the meso structure of the material of a body, the movement of dislocations and atoms of a material, the interaction of elementary particles and so on. Usually it is not constructive to incorporate the local behavior of a specific scale in a higher scale, e.g. the attempt of describing the movement of galaxies by including the behavior of all the individual atoms in the modeling approach would be unreasonable, even though it might be possible in general. The usual approach in physics is to make an experiment (sometimes

replaced by simulations) on the desired scale to get an effective behavior, even if it is known, that this effective behavior depends on the structure and properties of the lower scales.

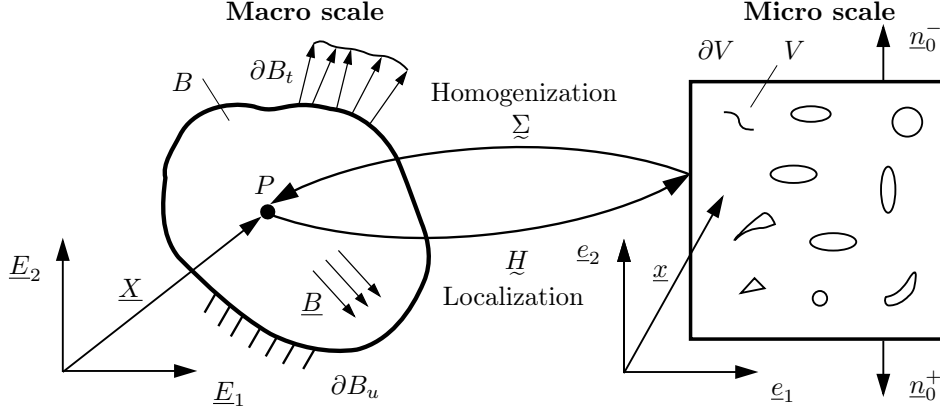


Figure 1: Mechanical two-level multiscale model: Localization of the locally uniform macroscopic deformation state, Homogenization of the inhomogeneous microscopic stress response

In material modeling the effective properties can be very complicated, especially when the material behavior is strongly irreversible and experiments might be very expensive and complicated. Since engineering materials are artificial, it's micro structure and the behavior of the individual components are sometimes well known and understood. Then the at the structural scale well approved Cauchy Continuum might be just applied at the micro scale (depending on the size also called meso scale). The multiscale problem is depicted in Figure 1. It is assumed that the macroscopic values of mechanical power, 1. Piola Kirchhoff stress and displacement gradient can just be defined as the volume average of their microscopic counterparts, whereat the first is known as "Hill-Mandel" or "macro homogeneity" condition:

$$P = J \underline{\Sigma} : \underline{D} = \underline{\Sigma}^{\text{PK}} : \underline{\dot{H}} = \langle p \rangle_0 = \langle \underline{\sigma}^{\text{PK}} : \underline{\dot{h}} \rangle_0 = \frac{1}{V_0} \int_{V_0} \underline{\sigma}^{\text{PK}} : \underline{\dot{h}} \, dV \quad (1)$$

$$\underline{\Sigma}^{\text{PK}} = \langle \underline{\sigma}^{\text{PK}} \rangle_0 = \frac{1}{V_0} \int_{V_0} \underline{\sigma}^{\text{PK}} \, dV = \frac{1}{V_0} \int_{\partial V_0} \underline{t} \otimes \underline{x}_0 \, dS \quad (2)$$

$$\underline{H} = \underline{U} \otimes \nabla_{\underline{X}_0} = \langle \underline{h} \rangle_0 = \frac{1}{V_0} \int_{V_0} \underline{h} \, dV = \frac{1}{V_0} \int_{\partial V_0} \underline{u} \otimes \underline{n}_0 \, dS \quad (3)$$

A RVE must be identified, being representative for the surrounding of a point  $P$ . The scale bridging is established in terms of Homogenization by the definition of the stress in form of the surface integral as shown in equation (2). The boundary value problem at the macro scale reads:

$$\text{div}(\underline{\Sigma}) + \underline{B} = \underline{\ddot{U}} \text{ in } B, \quad \underline{U} = \underline{\bar{U}} \text{ on } \partial B_u, \quad \underline{T} = \underline{\bar{T}} \text{ on } \partial B_t \quad (4)$$

The Localization step is introduced, by assuring that equation (3) is fulfilled apriori through suitable boundary conditions, whereby usually periodic boundary conditions are chosen, which assume a periodic RVE continuation by identifying homologous points  $()^+$  and  $()^-$ . All together the microscopic boundary value problem reads:

$$\text{div}(\underline{\sigma}) = \underline{0} \text{ in } V, \quad \underline{u}^+ - \underline{u}^- = \underline{H} \cdot [\underline{x}_0^+ - \underline{x}_0^-] \text{ on } \partial V \text{ with } \underline{n}_0^- = -\underline{n}_0^+ \quad (5)$$

The partial differential equations of the involved problems must be solved numerically, usually by means of the FEM. The discretized equilibrium equations of the macro problem in residual form read:

$$\hat{R}(\hat{U}, \hat{u}) = \underbrace{\sum_{\alpha=1}^i \underline{B}_{\alpha}^T \cdot \underline{\Sigma}_{\alpha}(\hat{U}, \hat{u}_{\alpha})}_{\hat{F}_{\text{int}}} - \hat{F}_{\text{ext}} + \hat{F}_{\text{kin}}(\hat{U}) = \underline{0} \quad (6)$$

Thereby all measures with  $(\hat{\cdot})$  denote nodal values. The numerical integration interrogates the stress response of an attached RVE at all integration points  $\alpha$  from 1 to  $i$ . The projection onto the global B-Matrix yields the vector of internal Forces. At the micro scale the discretized FEM equations read for one macroscopic integration point  $\alpha$ :

$$\hat{u}_{\alpha}^{-}(\hat{u}_{\alpha}, \underline{H}_{\alpha}) = \underline{A} \cdot \begin{bmatrix} \hat{u}_{\alpha} \\ \underline{H}_{\alpha} \end{bmatrix}, \quad \hat{u}_{\alpha} = \begin{bmatrix} \hat{u}_{\alpha}^+ \\ \hat{u}_{\alpha}^{\text{inner}} \end{bmatrix}, \quad \hat{r}(\hat{U}, \hat{u}_{\alpha}) = \hat{f}_{\text{int} \alpha} + \underline{A}^T \cdot \hat{f}_{\text{int} \alpha}^{-} = \left[ \underline{\Sigma}_{\alpha}^{\text{PK}} \cdot V_0 \right] \quad (7)$$

Therein a matrix  $\underline{A}$  is introduced giving the linear relation (5) between the displacement of the “-” nodes and the displacement of the “+” nodes and the macro displacement gradient. The superscript <sup>inner</sup> corresponds to the nodes which are not a the boundary. The Galerkin projection for the “-” internal force with  $\underline{A}$  then reflects the fact that  $\underline{t}^- = -\underline{t}^+$  and that the force response to the macro displacement gradient will be the macro stress.

### 3. Solution strategy

#### 3.1. General aspects

In the last decades a lot of material formulations have emerged. For now we want to compare them in a rough sense in terms of flexibility and computational efficiency, assuming all methods to be as accurate as needed for engineering purposes. The optimal material formulation would be flexible to account for any type of material, while needing as few computational resources as possible cf. Figure 2 (a). As shown in Figure 2 (b) the effort in modeling can be classified into online costs, which include all needed resources for the actual simulations, offline costs, which include possible training data generation and evaluation and adaptation effort, which comprises all necessary steps to adapt or develop a method to account for a specific material behavior.

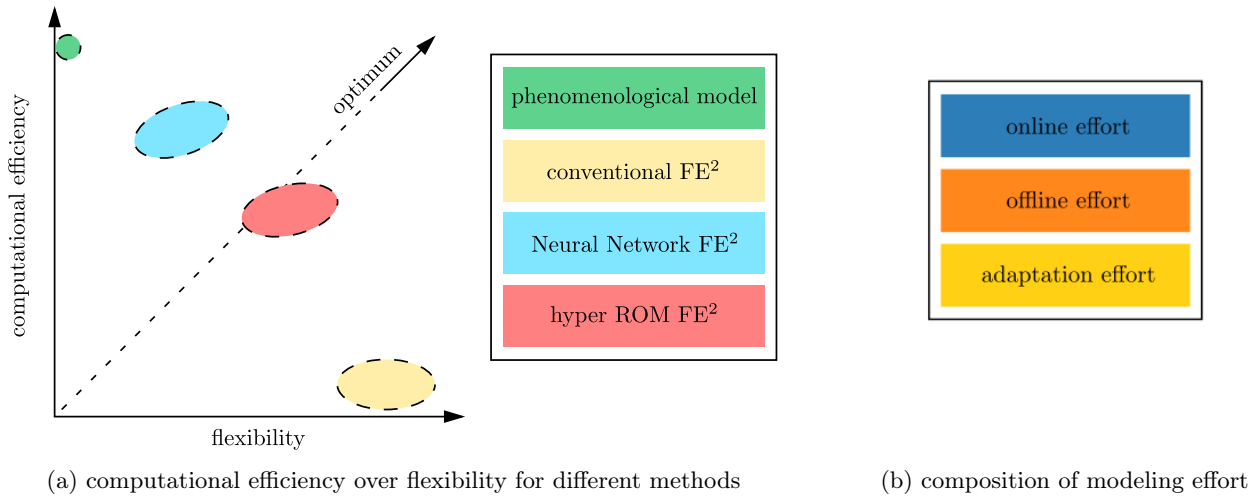


Figure 2: general classification of formulations for materials with characteristic micro structure

Classical phenomenological material descriptions, sometimes being micromechanically motivated like the GTN model for porous metals or the Deshpande Fleck model form Foams, are often very efficient, while only being able to capture the effects of specific materials. On the contrast the conventional FE<sup>2</sup> method, in this context often referred to as High Fidelity (HF) model, is theoretically able to account for any type of material, though being so computationally inefficient, that it may never leave the academic context. In order to speed up the FE<sup>2</sup> process, often Neuronal Network based material formulations are developed, which use RVE-FE training data as input. They are shown to save a lot of computational costs in the online phase [38]. However they need a lot of training data, since Neuronal Network do not inter- and extrapolate well and they lose track to the original PDE, wherefore specific considerations must be taken into account to get a physically consistent response [27] (=adaptation effort). That usually leads to formulations, which may be able to account for a broader spectrum of problems then classical material descriptions, but are much more restricted then the conventional FE<sup>2</sup> method. The hyper ROM FE<sup>2</sup> still solves the PDE and shows to extra- and interpolate well in untrained regions, whereby it generally needs less training data and no adaptation effort is necessary to account for specific material behavior. However the online costs are usually higher as those of Neuronal Network based models [38].

## 3.2. Reduced Order Modeling

### 3.2.1. Foundations

Reduced Order Modeling is a class of techniques used quite frequently in a lot of different fields of application. Its main idea lies in the observation that many problems containing a lot of information can usually be described with very good accuracy by so called lower order approximations, because the grade of correlation is high. In particular regarding the recent trend of gathering more and more data, often the problem of evaluating this data in reasonable time respectively to store the information in a compressed way arises. The roots go back to the 19<sup>th</sup> century, whereby depending on the field of application different names for the same/similar technique are established for decomposing large amounts of discrete data with a large amount of coherence, including Proper Orthogonal Decomposition (POD), Singular Value Decomposition (SVD), Principal Component Analysis (PCA), Karhunen-Loeve Transforma (KLT), Hotelling Transform among others. A broad overview can be found in [2].

Regarding a (discrete) mechanical problem, where the value of the nodal displacements  $\hat{\underline{u}}(t) \in \mathbb{R}^{\hat{n}}$  of a RVE at time  $t$  are being sought, this kind of approach leads to linear combinations of orthonormal basis vectors  $\underline{\phi}_i \in \mathbb{R}^{\tilde{n}}$   $i = 1, \dots, \tilde{n}$  with  $\tilde{n} \ll \hat{n}$ , yielding

$$\hat{\underline{u}}(t) \approx \underline{\phi} \cdot \tilde{\underline{u}}(t) , \quad (8)$$

whereby  $\tilde{\underline{u}} \in \mathbb{R}^{\tilde{n}}$  are the amplitudes of the corresponding basis vectors. The basis vectors  $\underline{\phi}_i$  can be interpreted as deformation modes, whereby only the most dominant ones are being considered. The modes can be found through a SVD applied to a collection of displacement snapshots from RVE simulations using representative loading paths, yielding the matrix decomposition as shown in equation (9). Thereby an elastic-inelastic-split as proposed in [16] should be used, which assures that the elastic range is recovered exactly:

$$\hat{\underline{\underline{x}}}_u^{\text{el}} = \underline{\phi}^{\text{el}} \cdot \underline{\underline{\Sigma}}_u^{\text{el}} \cdot \underline{\underline{V}}_u^{\text{elT}} , \quad \hat{\underline{\underline{x}}}_u^{\text{inel mod}} = \underline{\phi}^{\text{inel}} \cdot \underline{\underline{\Sigma}}_u^{\text{inel}} \cdot \underline{\underline{V}}_u^{\text{inelT}} , \quad \underline{\phi} = \begin{bmatrix} \underline{\phi}^{\text{el}} & \underline{\phi}^{\text{inel}} \end{bmatrix} \quad (9)$$

Here  $\hat{\underline{\underline{x}}}_u$  contains the value of the nodal displacements at selected points of time from each training load case:

$$\hat{\underline{\underline{x}}}_u^{\text{el}} = \left[ \hat{\underline{u}}^{\text{el}1}, \hat{\underline{u}}^{\text{el}2}, \dots \right] , \quad \hat{\underline{\underline{x}}}_u^{\text{inel}} = \left[ \hat{\underline{u}}^{\text{inel}1}, \hat{\underline{u}}^{\text{inel}2}, \dots \right] , \quad \hat{\underline{\underline{x}}}_u^{\text{inel mod}} = \hat{\underline{\underline{x}}}_u^{\text{inel}} - \underline{\phi}^{\text{el}} \cdot \underline{\phi}^{\text{elT}} \cdot \hat{\underline{\underline{x}}}_u^{\text{inel}} \quad (10)$$

From equation (8) follows for the Galerkin Method for the nodal coefficients of the test field  $\delta \underline{u}(\underline{x})$

$$\delta \hat{\underline{u}}(t) \approx \underline{\phi} \cdot \delta \tilde{\underline{u}}(t) , \quad (11)$$

since the same ansatz is being made for the actual and test displacement field. Considering the virtual work of an RVE assuming a quasi-static problem with a divergence free stress field this leads to

$$\delta w = 0 = \delta \hat{\underline{u}}^{\text{T}} \cdot \int_V \underline{\underline{B}}^{\text{T}} \cdot \underline{\sigma} \, dV = \delta \hat{\underline{u}}^{\text{T}} \cdot \underline{\underline{f}}^{\text{int}} = \delta \hat{\underline{u}}^{\text{T}} \cdot \underline{\hat{r}} = \delta \tilde{\underline{u}}^{\text{T}} \cdot \underline{\phi}^{\text{T}} \cdot \underline{\hat{r}} = \delta \tilde{\underline{u}}^{\text{T}} \cdot \underline{\tilde{r}} . \quad (12)$$

The linearization of equation (12) yields

$$\frac{d \underline{\tilde{r}}}{d \underline{\tilde{u}}} = \frac{d \underline{\tilde{r}}}{d \underline{\hat{r}}} \cdot \frac{d \underline{\hat{r}}}{d \underline{\hat{u}}} \cdot \frac{d \underline{\hat{u}}}{d \underline{\tilde{u}}} = \underline{\phi}^{\text{T}} \cdot \underline{\hat{k}} \cdot \underline{\phi} = \underline{\tilde{k}} , \quad (13)$$

whereby  $\underline{\tilde{k}}$  becomes a dense matrix.

### 3.2.2. Large deformations

When at large deformations, additionally to a deformation, a rigid body rotation is superimposed onto an RVE, either the rotations must be trained, by selecting the deformation gradient as strain measure as proposed in [3], or training directions that do not contain macroscopic rigid body motion are chosen, requiring the basis system to be rotated along in the online stage, since the ROM basis is then defined in an unrotated configuration. This however may be impractical and time consuming in an actual implementation. Rather it seems promising to only impose the stretch onto the RVE and get the (symmetric) Biot stress as response. Working with these symmetric stress/strain measures additionally has the advantage of lowering the computational effort in computing the (macro) stress and condensing the tangent (in 3D only 6 instead of 9 independent variables), which was also observed by Kochmann et al. [24] and no macroscopic rotations have to be trained. Additionally

it makes a code with little effort compatible for both small and large deformation theory. At first consider the polar decomposition of the deformation gradient and the velocity gradient as shown in equation (14)

$$\underline{F} = \underline{I} + \underline{H} = \underline{R} \cdot \underline{U}, \quad \underline{L} = \dot{\underline{F}} \cdot \underline{F}^{-1} = \underline{D} + \underline{W} = \underbrace{\underline{R} \cdot \text{sym}(\dot{\underline{U}} \cdot \underline{U}^{-1}) \cdot \underline{R}^T}_{\underline{D}} + \underbrace{\dot{\underline{R}} \cdot \underline{R}^T + \underline{R} \cdot \text{skw}(\dot{\underline{U}} \cdot \underline{U}^{-1}) \cdot \underline{R}^T}_{\underline{W}} \quad (14)$$

where  $\underline{R}$  is the macro rotation,  $\underline{U}$  the right stretch,  $\underline{D}$  the rate of deformation and  $\underline{W}$  the spin tensor. Considering the mechanical power it can be shown that  $\dot{\underline{U}}$  is work conjugate to the (symmetric) Biot stress  $\underline{\Sigma}^B$  as shown in equation (15).

$$J \underline{\Sigma} : \underline{D} = J \underline{\Sigma} : \underline{R} \cdot \text{sym}(\dot{\underline{U}} \cdot \underline{U}^{-1}) \cdot \underline{R}^T = \text{sym}(\underline{R}^T \cdot J \underline{\Sigma} \cdot \underline{F}^{-T}) : \dot{\underline{U}} = \underline{\Sigma}^B : \dot{\underline{U}} \quad (15)$$

Since a lot of commercially available FE codes, like Abaqus, Ansys etc. work with the true (Cauchy) stress, the output in terms of stress and tangent must be transformed by using a push forward operation. Considering equation (15) the Cauchy stress can therewith be written as a function of the Biot stress as shown in equation (16).

$$\underline{\Sigma}^B = \frac{J}{2} [\underline{R}^T \cdot \underline{\Sigma} \cdot \underline{F}^{-T} + \underline{F}^{-1} \cdot \underline{\Sigma} \cdot \underline{R}] \leftrightarrow \underline{\Sigma} = \frac{2}{J} [R_{ik} F_{lj}^{-1} + F_{ki}^{-1} R_{jl}]^{-1} \Sigma_{kl}^B \underline{e}_i \otimes \underline{e}_j \quad (16)$$

In the appendix A it is shown how to compute the necessary algorithmically consistent tangent as required in the Update Lagrange context.

### 3.2.3. Monolithic solution scheme

The numerical treatment in solving equation (12) follows in analogy to the full problem. Regarding the previously by the authors proposed monolithic scheme [25] as shown in Figure 3 (b) the only change is in using amplitudal quantities in stead of nodal ones at the micro scale. For the increment of the microscopic nodal displacements this yields

$$\Delta \underline{\tilde{u}} = - \left[ \underline{\phi}^T \cdot \underline{\hat{k}} \cdot \underline{\phi} \right]^{-1} \cdot \left[ \underline{\phi}^T \cdot \underline{\hat{r}} + \underline{\phi}^T \cdot \frac{\partial \underline{\hat{r}}}{\partial \underline{U}} \cdot \Delta \underline{U} \right] = - \underline{\tilde{k}}^{-1} \cdot \left[ \underline{\tilde{r}} + \frac{\partial \underline{\tilde{r}}}{\partial \underline{U}} \cdot \Delta \underline{U} \right]. \quad (17)$$

The algorithmic consistent macroscopic (Biot) stress can be computed as

$$\underline{\Sigma}_{\text{alg}}^B = \underline{\Sigma}^B - \frac{\partial \underline{\Sigma}^B}{\partial \underline{\hat{u}}} \cdot \underline{\phi} \cdot \left[ \underline{\phi}^T \cdot \underline{\hat{k}} \cdot \underline{\phi} \right]^{-1} \cdot \underline{\phi}^T \cdot \underline{\hat{r}} = \underline{\Sigma}^B - \frac{\partial \underline{\Sigma}^B}{\partial \underline{\tilde{u}}} \cdot \underline{\tilde{k}}^{-1} \cdot \underline{\tilde{r}}. \quad (18)$$

The tangent stiffness in terms of amplitudal quantities reads

$$\underline{\underline{C}}^B = \frac{\partial \underline{\Sigma}^B}{\partial \underline{U}} - \frac{\partial \underline{\Sigma}^B}{\partial \underline{\hat{u}}} \cdot \underline{\phi} \cdot \left[ \underline{\phi}^T \cdot \underline{\hat{k}} \cdot \underline{\phi} \right]^{-1} \cdot \underline{\phi}^T \cdot \frac{\partial \underline{\hat{r}}}{\partial \underline{U}} = \frac{\partial \underline{\Sigma}^B}{\partial \underline{U}} - \frac{\partial \underline{\Sigma}^B}{\partial \underline{\tilde{u}}} \cdot \underline{\tilde{k}}^{-1} \cdot \frac{\partial \underline{\tilde{r}}}{\partial \underline{U}}. \quad (19)$$

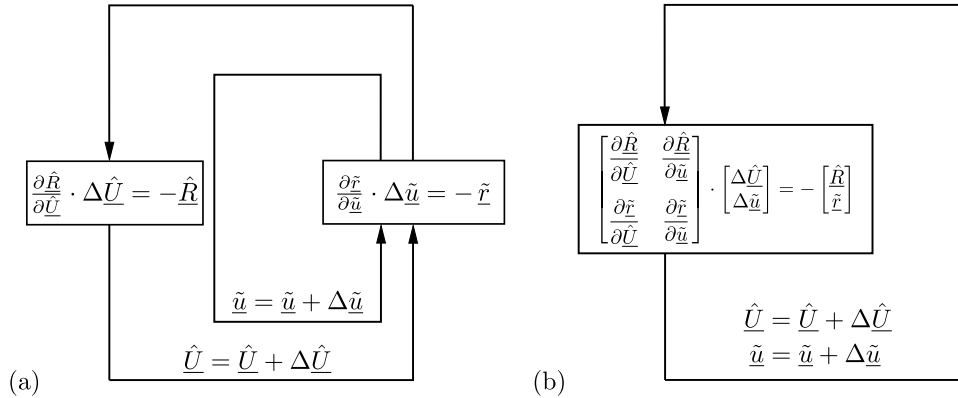


Figure 3: (a) staggered algorithm, (b) monolithic algorithm, see also [25]

### 3.3. Hyper integration

The result of section 3.2 in terms of computational efficiency is that only a small number of  $\tilde{n}$  equations have to be solved compared to the large number of  $\hat{n}$  DOF of the full system. However computing the integral of equation (12), as well as computing the macroscopic stress is still very expensive, besides the projection with  $\underline{\underline{\phi}}$  introduces additional computational effort.

There are mainly two integration methods described in literature, which are Empirical Interpolation Methods (EIM) and Empirical Cubature Methods (ECM) [16], [46]. A numerical examination in comparing different approaches in the multiscale context can be found e.g. in [46] and [44]. Tuijl et.al. conclude, that even though EIM methods lead to higher speedups, they tend to produce more interpolation errors and its less straightforward to construct accurate snapshots spaces in comparison to the in that regard more promising ECM methods [46]. In the scope of this work we will only focus on the ECM approach.

In the context of multiscale modeling, Hernández et al. were the first to comprehensively elaborate the ECM to the needs of the FE<sup>2</sup> method [16], whereby the idea traces back to the work of An et al. [1]. An overview of further roots can be found in [15]. Subsequently the algorithm was applied by different authors e.g. [39], [46] and developed further to e.g. the reduced energy optimal cubature REOQ [3],[37] which relies on the integration of the free energy, which however cannot be applied to by the authors preferred hypoelastic material formulations in a straightforward manner. Hernández later applied the method to general periodic structures [14], which represents an effective tool for weak scale separations, but cannot be reasonably applied for large scale separations. An interesting work of Rocha et al. [40] shows an offline-free adaptive ROM/ECM implementation, which does not need a training stage, but shows less online speedup than the original method of Hernández et al.

The principal idea of the ECM is to find a set of  $\tilde{m}$  integration points ( $\tilde{m} \ll m$ ) such that

$$\underline{\underline{f}}^k = \left[ \underline{\underline{\phi}}^T \cdot \int_V \underline{\underline{B}}^T \cdot \underline{\underline{\sigma}} dV \right]^k = \left[ \int_{V_0} \frac{1}{j} \cdot \underline{\underline{\phi}}^T \cdot \underline{\underline{B}}^T \cdot \underline{\underline{\sigma}} dV \right]^k \approx \sum_{g=1}^m w^g \underline{\underline{f}}^{k g} \approx \sum_{g=1}^{\tilde{m}} \tilde{w}^g \underline{\underline{f}}^{k g}, \quad \text{with } \underline{\underline{f}}^g = \underline{\underline{f}}(\tilde{x}^g) \quad (20)$$

for all  $k = 1, \dots, p$  snapshots. Preferably an integral over the reference domain should be pursued for finite deformations, so that the weights remain constant. In finding the hyper integration points under the points of the HF integration  $\tilde{z} = \{\tilde{x}^g\}_{g=1}^{\tilde{m}} \subset z$  and their associated positive weights  $\tilde{w} = [\tilde{w}^1, \tilde{w}^2, \dots, \tilde{w}^g]^T$ , an optimization problem is formulated and transferred to matrix notation for being feasible for a computer implementation, which reads

$$(\tilde{w}, \tilde{z}) = \arg \min_{\substack{\tilde{w} \in \mathbb{R}_+^{\tilde{m}}, \\ \tilde{z} \subset z}} \left( \left\| \sum_{k=1}^p \sum_{i=1}^{\tilde{n}_t} \sum_{g=1}^{\tilde{m}} \tilde{w}^g \tilde{f}_i^{k g} - f_i^k \right\|^2 + \left\| \sum_{g=1}^{\tilde{m}} \tilde{w}^g - V_0 \right\|^2 \right) = \arg \min_{\substack{\tilde{w} \in \mathbb{R}_+^{\tilde{m}}, \\ \tilde{z} \subset z}} \left\| \begin{bmatrix} \tilde{z} \\ \mathbf{1} \end{bmatrix} \cdot \tilde{w} - \begin{bmatrix} \mathbf{0} \\ V_0 \end{bmatrix} \right\| \quad (21)$$

with the training matrix  $\underline{\underline{x}}_f$

$$\underline{\underline{x}}_f = \begin{bmatrix} \tilde{f}_1^{11} - \tilde{f}_1^1/V_0 & \tilde{f}_1^{12} - \tilde{f}_1^1/V_0 & \dots & \tilde{f}_1^{1m} - \tilde{f}_1^1/V_0 \\ \tilde{f}_2^{11} - \tilde{f}_2^1/V_0 & \tilde{f}_2^{12} - \tilde{f}_2^1/V_0 & \dots & \tilde{f}_2^{1m} - \tilde{f}_2^1/V_0 \\ \dots & \dots & \vdots & \dots \\ \tilde{f}_{\tilde{n}_t}^{p1} - \tilde{f}_{\tilde{n}_t}^p/V_0 & \tilde{f}_{\tilde{n}_t}^{p2} - \tilde{f}_{\tilde{n}_t}^p/V_0 & \dots & \tilde{f}_{\tilde{n}_t}^{pm} - \tilde{f}_{\tilde{n}_t}^p/V_0 \end{bmatrix} \quad (22)$$

and including the fundamental requirement of every plausible integration scheme, which states that the volume has to be integrated exactly

$$\int_{V_0} 1 dV = \sum_{g=1}^m w^g = \sum_{g=1}^{\tilde{m}} \tilde{w}^g = V_0. \quad (23)$$

Thereby the number  $\tilde{n}_t$  equaling to  $\tilde{n}_t = \tilde{n} + n_\Sigma$  reflects the total number of global force values, with  $n_\Sigma$  being the distinct macroscopic stress components (3D:  $n_\Sigma = 6$ , 2D:  $n_\Sigma = 3$ ), compare equation (5), because in this formulation the total displacement field is included in  $\underline{\underline{\phi}}$  in contrast to the implementation of Hernández, in which  $\underline{\underline{\phi}}$  is a basis for the fluctuation field. This ensures, that the macroscopic stress will be integrated correctly.

Hernández et al. [16] cleverly applied a nonnegative greedy selection algorithm, to select the hyper points efficiently. In order to integrate the volume exactly and be able to efficiently carry out the selection algorithm,

instead of using the training matrix  $\underline{x}_f$  directly, a SVD is applied thereon as shown in equation (24), since a high grade of correlation can be observed therein.

$$\underline{x}_f^T = \underline{\lambda} \cdot \underline{\Sigma}_f \cdot \underline{V}_f^T \quad \text{and} \quad \underline{x}_f \cdot \underline{\tilde{w}} = \underline{V}_f \cdot \underline{\Sigma}_f^T \cdot \underbrace{\left[ \underline{\lambda}^T \cdot \underline{\tilde{w}} \right]}_{\approx \underline{0}} \approx \underline{0} \quad (24)$$

This comes with the important side effect, that  $\underline{\lambda}$  is a unitary matrix and the greedy algorithm will select an optimal result for the information given in  $\underline{\lambda}$ , when it is truncated to  $\tilde{m} - 1$  rows. The overall algorithm is summarized in box 1.

**Inputs:**  $\underline{j} = \left[ \underline{\lambda} \quad \underline{1} \right]^T$ ,  $\underline{b} = \left[ \underline{0}^T \quad V \right]^T$

**Starting values:**

- The set containing hyper integration points:  $\underline{\tilde{z}} = \emptyset$
- The set of available points:  $\underline{y} = \underline{z}$
- The number of already chosen (positive) weights  $\underline{\tilde{w}}$ :  $\tilde{m}_+ = 0$
- The residual vectors:  $\underline{r} = \underline{b}$

**while**  $\tilde{m}_+ < \tilde{m}$  **do:**

1. Compute next hyper point:  $k = \arg \max_{k \in \underline{y}} \left\{ \underline{j}_k \cdot \underline{r} / \|\underline{j}_k\| \right\}$
2. Put  $k$  into  $\underline{\tilde{z}}$  and remove it from  $\underline{y}$  ( $\underline{\tilde{z}} = \underline{\tilde{z}} \cup k$ ,  $\underline{y} = \underline{y} \setminus k$ )
3. Determine  $\underline{\tilde{w}}$  by unrestricted least square (`numpy.linalg.lstsq`)

$$\underline{\tilde{w}} = \min \left\| \underline{j}^{\underline{\tilde{z}}} \cdot \underline{\tilde{w}} - \underline{b} \right\|$$

4. If all entries of  $\underline{\tilde{w}}$  are nonnegative go to step 7.
5. Determine  $\underline{\tilde{w}}$  by applying nonnegative least squares (`scipy.optimize.nnls`)

$$\underline{\tilde{w}} = \arg \min_{\underline{\tilde{w}} > 0} \left\| \underline{j}^{\underline{\tilde{z}}} \cdot \underline{\tilde{w}} - \underline{b} \right\|$$

6. Set  $\underline{\tilde{z}} = \underline{\tilde{z}} \setminus \underline{\tilde{z}}_0$  with  $\underline{\tilde{z}}_0 = \underline{\tilde{z}}_0 \cup \{g \mid g \in \underline{\tilde{z}} \wedge \tilde{w}^g = 0\}$ ,  $\underline{\tilde{w}} = \underline{\tilde{w}}(\underline{\tilde{z}})$ , with  $\underline{z}_0$  being a set of excluded points with zero weight
7. Compute the residual  $\underline{r} = \underline{j}^{\underline{\tilde{z}}} \cdot \underline{\tilde{w}} - \underline{b}$  and set  $\tilde{m}_+ = \text{card}(\underline{\tilde{z}})$

**end**

Box 1.: Empirical cubature method (offline stage). Greedy algorithm for computing an optimal set of integration points  $\underline{\tilde{z}} = 1, 2, \dots, \tilde{m}$  and corresponding weights  $\underline{\tilde{w}} \in \mathbb{R}_+^{\tilde{m}}$ . (after [15])

### 3.4. Clustered training trajectories

The hyper ROM method relies on an “offline” (“training”) phase to gather the matrices  $\hat{\underline{x}}_u$  and  $\underline{x}_f$  with nodal displacements and integration point forces respectively. Thereby a set  $\mathbb{T}$  with stress  $\underline{\Sigma}(t)$  and displacement gradient  $\underline{H}(t)$  trajectories

$$\mathbb{T} = \{ \underline{\Sigma}_1(t), \underline{\Sigma}_2(t), \dots, \underline{H}_1(t), \underline{H}_2(t), \dots \} \quad (25)$$

must be found. Finding a good training set is a non trivial task. The optimal set would include as few trajectories as possible, while the therewith generated snapshots are being representative for the macroscopic problem(s), so that they can be solved within a given accuracy. In terms of the ROM method this leads to the smallest basis  $\underline{\phi}$ , incorporating only modes being relevant for the problem(s).

The worst training scenario is a fine and “blind” training of e.g. the strain space. A negative example can be found e.g. in [30], where the training set for a 2D example comprises 10,000 trajectories. A more sophisticated, iterative training strategy for Neural Networks can be found e.g. in [22]. Therein starting from an initially small training set the macroscopic problem is being simulated, if new so far not trained paths are being found, the training set is enriched and after a Neural Network calibration process the problem is simulated again. This process is repeated until convergence is reached.

Since the hyper ROM method inter- and extrapolate very well in regions, which were not trained, we propose a process, where the desired structure is simulated at first using a simple replacement material model,

e.g. only linear elastic with the initial RVE stiffness. In force controlled problems, the stress field will often be not too far off from the actual problem, vice versa the strain field in displacement controlled problems. Even usually not accepted large errors will be conceptually no problem, because it only affects the training input, which may still yield good simulation results in view of the good inter- and extrapolation properties. Then the stress or strain paths at the macroscopic integration points must be clustered, to vastly reduce the training data amount and to minimize unnecessary recurrences. Clustering is a type of unsupervised learning strategy, an overview can be found e.g. in [13]. We use  $k$ -means clustering, going back to [29], which is frequently used and widely accepted. To find the necessary number of  $k$  trajectories the Elbow method or more distinct approaches may be applied. The algorithm is quickly summarized in Box 2.

1. Determine a suitable simple replacement material model.
2. Simulate the macroscopic structure of interest and collect the stress or strain paths at the integration points.
3. Apply the  $k$ -means algorithm in suitable manner on the data to get  $\mathbb{T}$ .
4. Collect the training snapshots by simulating the RVE using the determined training trajectories and evaluate the data to get  $\underline{\phi}$ ,  $\underline{\tilde{z}}$  and  $\underline{\tilde{w}}$ .
5. Simulate the structure(s) of interest.
6. While stress/strain paths occur, which are too far off from the ones trained, go back to step 3 to enrich the training base, otherwise “training convergence” is reached.

Box 2.: Clustered training algorithm

## 4. Implementation

The described theory was implemented to the commercial FE code Abaqus. The main idea is to use Abaqus on the macro scale and the already established lightweight self contained code called `MonolithFE2` on the micro scale [25]. On the one hand Abaqus is well tested and has a lot of built-in features and materialroutines, on the other hand Abaqus is not reentrant and for that matter it is also too inflexible to implement the hyper ROM method in a straightforward manner.

In Figure 4 a flowchart is shown, which briefly depicts the main sub processes of the program. All parts of the `MonolithFE2` Kernel are written in object-oriented FORTRAN 2003. Abaqus enters the code at a specific macroscopic integration point  $\alpha$  through the UMAT interface. Since the UMAT interface only supports state variables  $\underline{a}_\alpha$  to an extent of 10,000 float numbers and only provides data from the last converged step, a self written data management using Pointers had to be implemented.

To make Abaqus element and material routines compatible to Abaqus and therewith allow e.g. a testing of the respective routines independently in Abaqus, the UEL and UMAT interface is also used within `MonolithFE2`.

The systems of equations are solved using the highly optimized INTEL `one api` MKL package. In HF simulations the PARDISO solver is used for LU-factorizing the sparse matrix, which uses an efficient supernodal method. In ROM simulations the GETRF/S solver is applied, which relies on Toledo’s recursive LU algorithm. It is worth mentioning that the inverses which appear in the text and the flowcharts are only written in favor of a slight notation, the inverses are never actually being calculated, rather the LU factorization is utilized together with the respective right hand sides.

Since the FE<sup>2</sup> method parallelizes very well, parallelization becomes a indisputable necessity regarding the high computational cost especially for industrial applications, wherefore the program was designed to run in parallel on shared as well as on distributed memory systems.

Postprocessing in the FE<sup>2</sup> method becomes a real issue, because in the HF method very large amounts of data emerge. In the hyper ROM method fewer data will be created, however to know the values of interest at all microscopic integration points, elaborate methods like Gappy Data Reconstruction would have to be employed. From a practical perspective and in view that often the homogenized macroscopic values are of interest, it seems

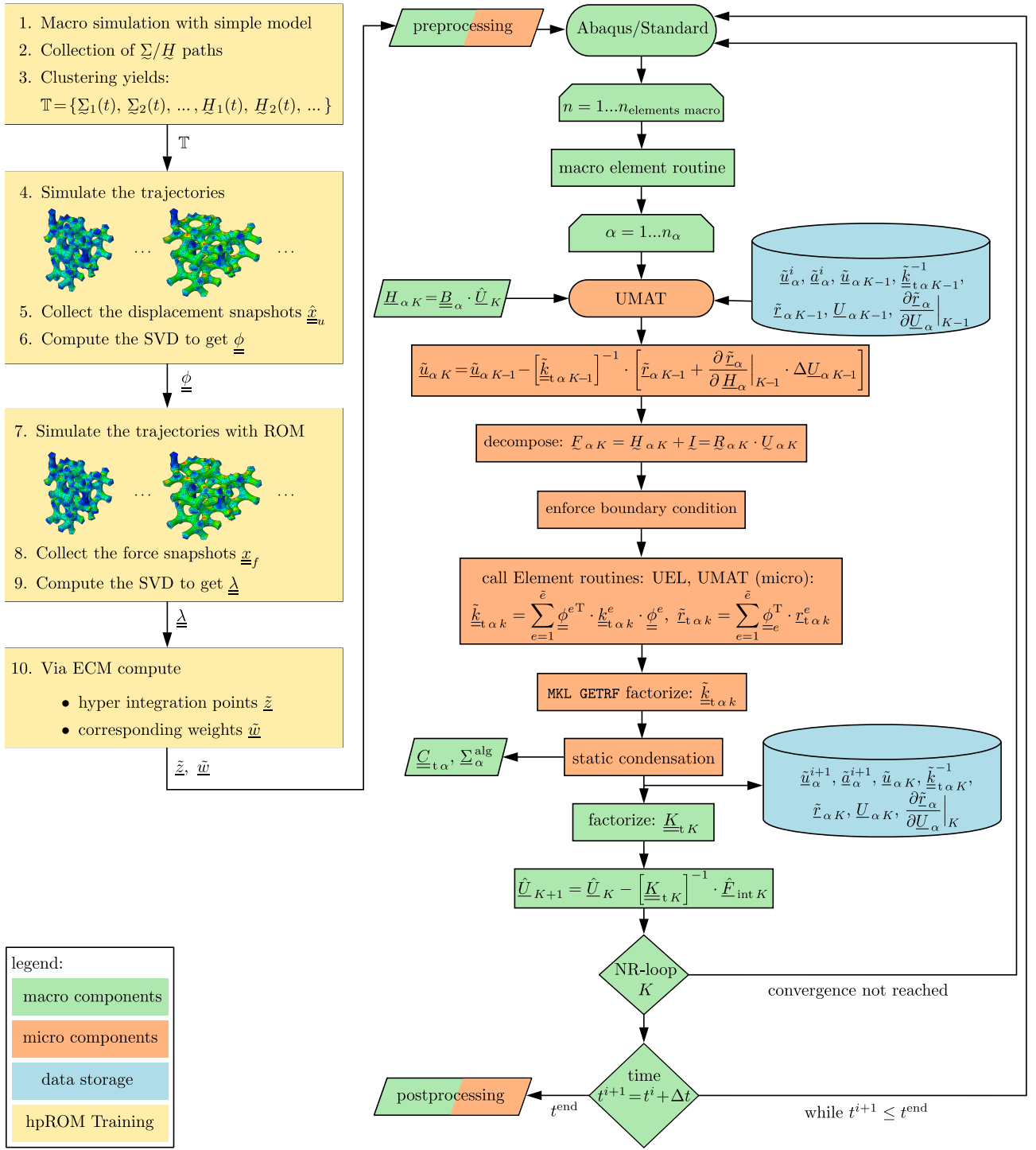


Figure 4: flowchart with the main online and offline steps of the monolithic hyper ROM method in MonolithFE<sup>2</sup>

to be more promising, to postprocess selected RVEs by imposing the strain history and perform a resimulation after the actual simulation.

To generate training data, the trajectories are defined in an input file for a Driver Program, which access MonolithFE<sup>2</sup> in parallel. Thereby the displacement at the nodes  $\hat{\underline{u}}$ , which are not constrained and the internal force  $\hat{\underline{f}}$  of the integration points are written to plain text files. Thereafter a Python script conducts the hyper ROM data evaluation. The computationally intensive parts, which operate with large matrices are written in FORTRAN 2003 and wrapped to Python. Reading the raw data from file and processing it to its final matrix Representation (see  $\hat{\underline{x}}_u$  and  $\underline{x}_f$ ) is done in parallel using openMP. The singular value decomposition of the respective matrices is computed using the INTEL one api MKL package GESVD, which also can be parallelized, even on distributed memory systems. The modified ECM algorithm is written in Python with aid of the numpy package linalg.lstsq and the scipy package optimize.nnls for unrestricted resp. nonzero-restricted least

square. The results in terms of the displacement modes  $\underline{\underline{\phi}}$  and hyper integration points  $\underline{\underline{\tilde{z}}}$  and corresponding weights  $\underline{\underline{\tilde{w}}}$  are written to the `MonolithFE2` input file.

Regarding the hyper ROM method, the programming is a compromise of being efficiently on the one side and on the other hand keeping the interventions in the classical HF code as little as possible and therewith preserving the modularity, since otherwise a lot of code doing essentially the same from the mathematical standpoint just for the sake of efficiency would have to coexist beside each other, making the code maintenance hard. In an actual online ROM simulation at first the full field of nodal displacements  $\underline{\underline{u}}$  is recovered from the ROM amplitudes  $\underline{\underline{\tilde{u}}}$ . In a ROM simulation with full integration, first the full vector of internal force and corresponding stiffnessmatrix in the CSR format (enables sparse matrix multiplication) is assembled and afterwards projected onto the modes. In the hyper integration mode only the elements having at least one integration point are called and on their part call the hyper element integration points. Only for these integration points memory is allocated to save the internal state variables  $\underline{\underline{q}}$ . Now the full internal force vector and tangent stiffness is not build up for reasons of efficiency. Rather the projection onto the modes follows directly with element ROM modes  $\underline{\underline{\phi}}^e$ , which are essentially just the rows of  $\underline{\underline{\phi}}$  corresponding to respective DOFs of an element.

## 5. Numerical examples

### 5.1. General remarks

This section is intended to show, that the monolithic hyper ROM FE<sup>2</sup> method represents an accurate approximation to the conventional HF FE<sup>2</sup> method, while being computationally very efficient. Accuracy is understood in an engineering sense, whereby depending on the application, deviations of around 5% in macroscopic force and displacement measures can be allowed in typical applications, since usually many parameters entering a simulation also differ in this range. However we set the allowed deviation to the reference HF model to around 1% in terms of global results. All simulations were carried out in parallel on a Computer with 16 physical cores of 8 Intel(R) Xenon(R) Gold 6244 processors and a main memory of 768 Gb DDR4.

### 5.2. Example 1: porous beam under bending

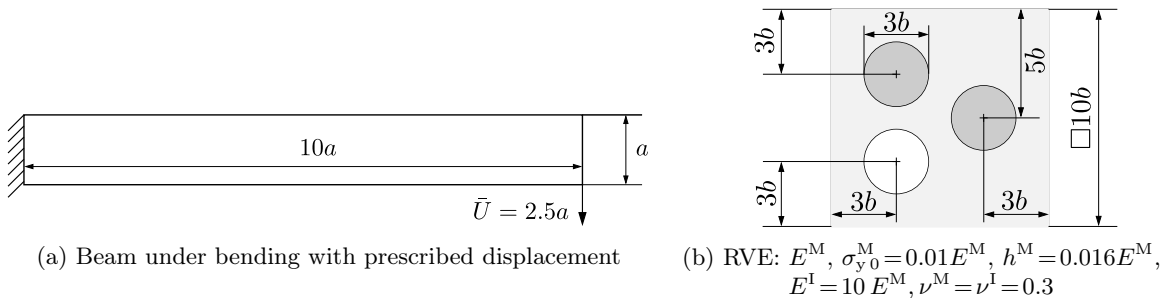


Figure 5: Example 1: Composite with soft elastic-plastic matrix and stiff elastic inclusions and a pore

In the first example the bending of a beam having a micro structure with a soft, elastic-plastic matrix with linear hardening, two elastic, stiff inclusions and one pore at plane strain condition and small deformations is simulated. The RVE is taken from a publication of Miehe and Koch [33]. The beams dimensions and boundary conditions are shown in Figure 5 (a). The RVE and its dimensions is shown in Figure 5 (b) together with the material parameters. Thereby  $()^M$  denotes Matrix properties and  $()^I$  those of the inclusions.

To apply the hyper ROM method efficiently and for the sake of a reasonable and fair comparison, first a convergence study should be performed. The RVE geometry was meshed with quadratic, triangular standard elements. The considered meshes are shown in Figure 6. To determine which mesh has an acceptable mesh quality, the test case of pure shear is considered. The macroscopic stress-strain curves are shown in Figure 7 (a). Taking Mesh (d) as the reference, the relative error of the macroscopic stress response is plotted in Figure 7 (b), proving the good mesh convergence of the used quadratic elements. Mesh (b) and (c) show macroscopic stress deviations w.r.t. to Mesh (d) of less then 1% error over the whole strain slope. By taking also the convergence of local field variables into account as can be seen in Figure 6, Mesh (c) was accepted and will be used in the subsequent investigations.

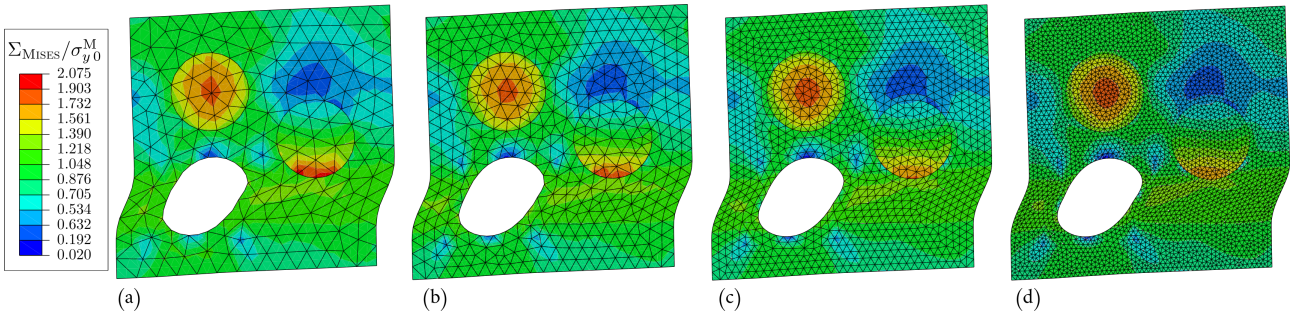
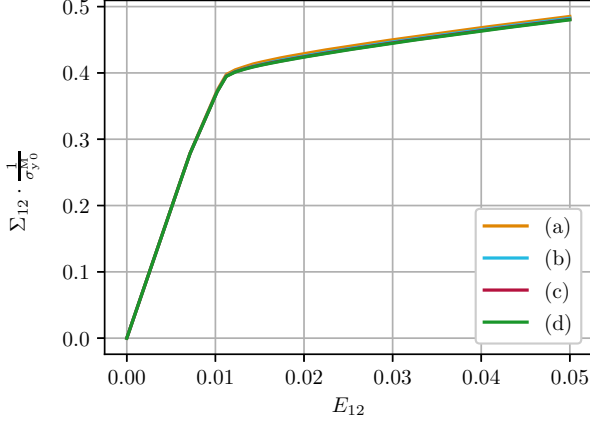
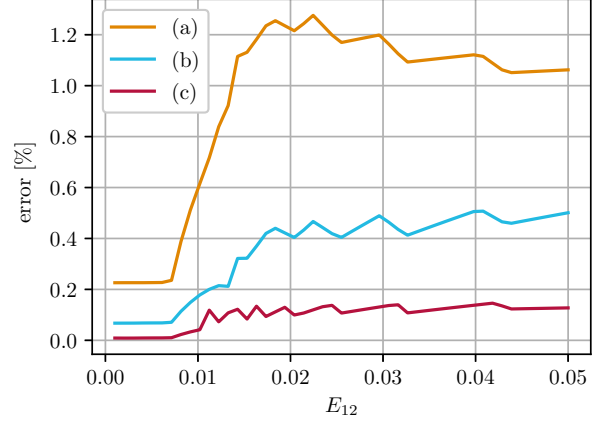


Figure 6: Considered meshes in the Mesh refinement examination

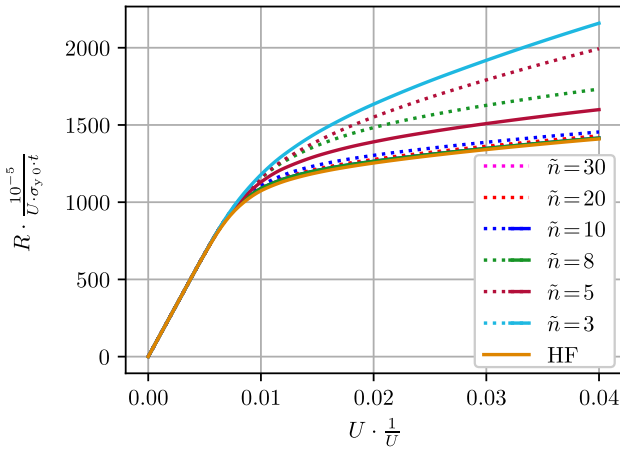


(a) stress-strain curves for Meshes (a)-(d)

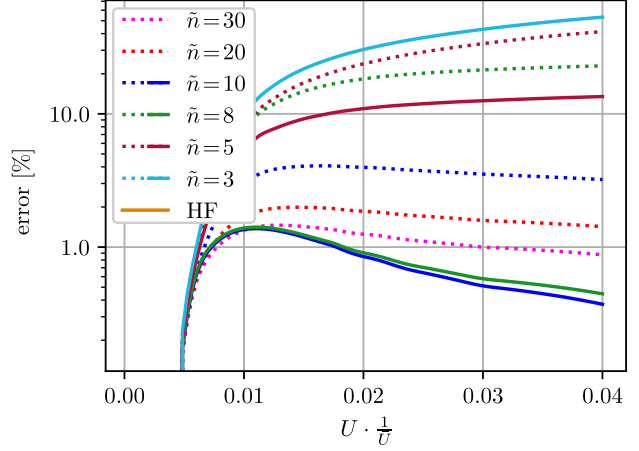


(b) Deviation of the stress values w.r.t. mesh (d)

Figure 7: Mesh convergence study Example 1



(a) force displacement curves for variation of  $\tilde{n}$



(b) relative error w.r.t. HF solution for variation of  $\tilde{n}$

Figure 8: ROM modes convergence study, solid lines: Clustered Training, dashed lines: unspecific Training

In the next step training trajectories must be chosen. To pursue the clustered training strategy, first a rough replacement material model must be found. In this case an isotropic MISES Plasticity model with Power law hardening is used, needing 4 Parameters, which are determined thorough one uniaxial tension simulation ( $E_{11} = 0.05$ ,  $\Sigma_{22} = \Sigma_{12} = 0.0$ ) to  $E = 1.01E^M$ ,  $\nu = 0.29$ ,  $\sigma_{y0}^M = 0.72 \sigma_{y0}^M$ ,  $N = 0.08$ , whereby the parameters are not optimized, but set by approximation formulas and experience. Then the Beam is simulated using this replacement model and the strain at all integration points is extracted from the last step. Afterwards the strain is normalized and clustered using a k-means clustering algorithm into 30 clusters. These 30 clusters are multiplied by the largest strain Frobenius norm of the beam model and then used as end values of monotonic, strain driven training simulations.

To find the necessary number of ROM modes to simulate Example 1 with sufficient accuracy, the beam

multiscale problem is simulated using an increasing number of ROM modes starting from the  $\tilde{n} = 3$  elastic modes up to  $\tilde{n} = 10$  modes and for comparison using the HF method. The global forces  $R$  over the prescribed displacement  $U$  is shown in Figure 8 (a) and its error w.r.t. the HF result is illustrated in Figure 8 (b). It can be asserted that with increasing the number of modes the ROM solution quickly converges towards the HF solution. Surprisingly already  $\tilde{n} = 8$  modes are capable of approximate the RVEs behavior with high accuracy. The proceeding of first simulate a problem full and the reduced to get the number of needed ROM modes is of course not practicable for real applications. It is shown for the sake of proving the convergence behavior of the ROM method. In actual applications, experience together with the testing of “representative” not trained trajectories are more suited to determine the necessary number  $\tilde{n}$ . To show the effect of the clustered training, an unspecific training strategy with 150 training trajectories was conducted (5 times more training trajectories  $\approx 5$  times more simulation effort). It can be seen from Figure 8, that it takes much more modes to converge to the HF result. This is the expected behavior, because the modes dominant in the unspecific training set, must not be the ones dominant in the actual structure. This shows empirically, that the clustered training does not only reduces the amount of training simulations, but also the number of necessary ROM modes.

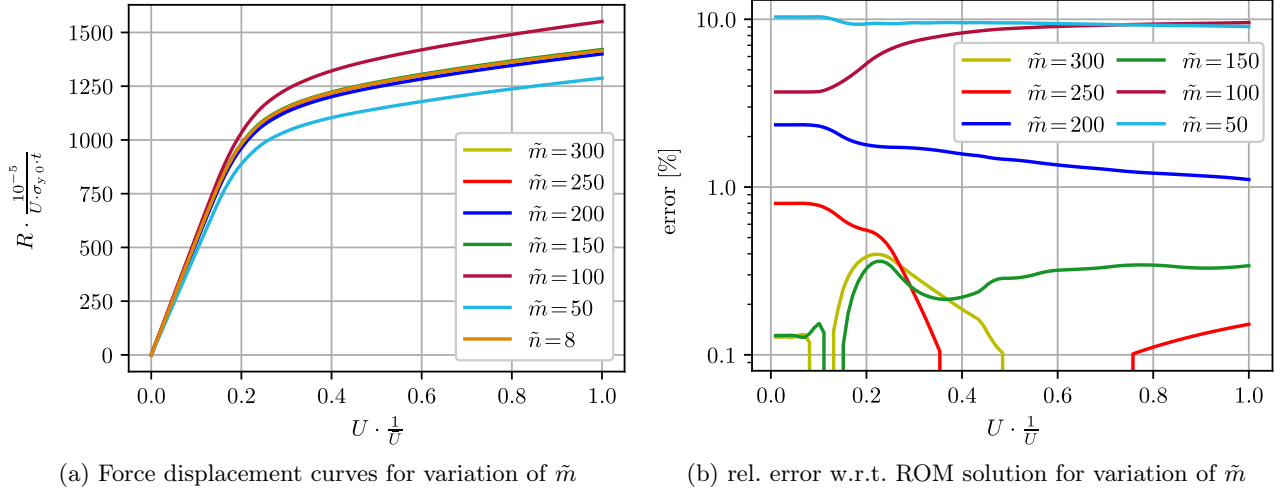


Figure 9: Hyper integration point convergence study for fixed number of  $\tilde{n} = 8$  modes

Subsequently the training trajectories were simulated again, now with the FE problem being restricted to 8 ROM modes. To find out how many hyper integration points are needed to describe example 1 with satisfactory accuracy, a convergence study is performed by increasing the number of hyper integration points starting from 50 in steps of 50. The global forces  $R$  over the prescribed displacement  $U$  is shown in Figure 9 (a) and its error w.r.t. the fully integrated ROM result is illustrated in Figure 9 (b). The solutions shows a convergence towards the HF solution with an increasing number of integration points. The hyper ROM model with  $\tilde{m} = 250$  shows deviations below 1% (globally) and will be consequently accepted as the final hyper ROM model.

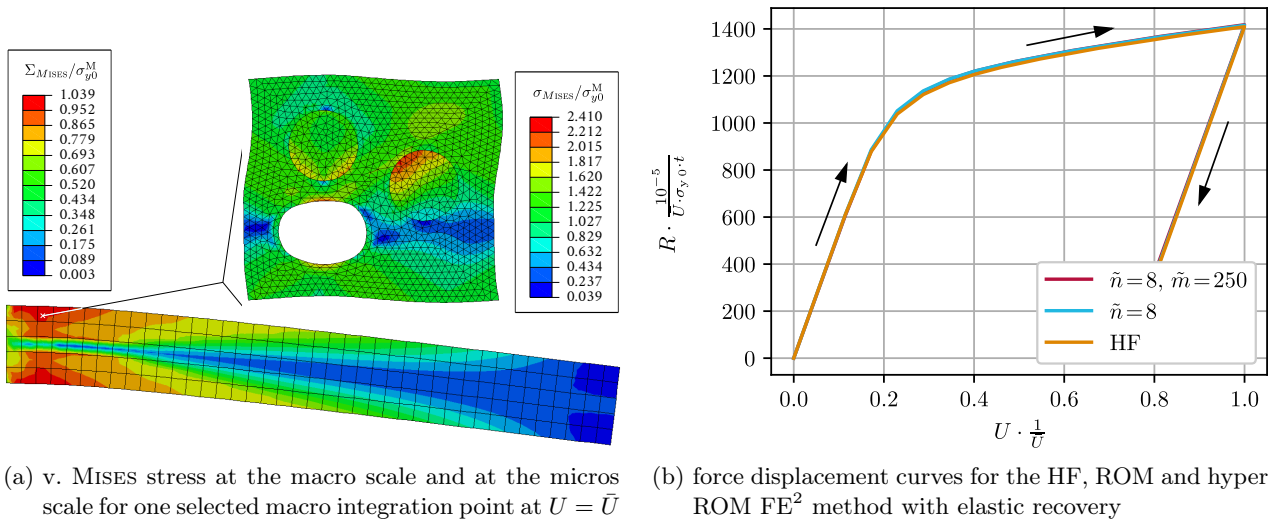


Figure 10: Final simulation result for beam bending of a composite

Finally Example 1 is simulated until  $\bar{U}$  is reached and then relieved until the global reaction force  $R$  is

returning to zero. Figure 10 (a) illustrates the MISES stress of the beam at  $U = \bar{U}$  and the MISES stress at the micro scale for a selected macro integration point. Figure 10 (b) shows the global reaction force over the prescribes displacement. It turns out that the ROM and hyper ROM FE<sup>2</sup> simulations predict the correct irreversible behavior, despite the fact that only monotonic training cases were considered.

Since the main objective of the hyper ROM method is to reduce the simulation effort in terms of needed simulation time, a respective examination is inquired. The results are illustrated in Figure 11, whereby the online time is plotted in blue and the offline time in orange. More details are shown in Table 1. It can be seen that the monolithic hyper ROM FE<sup>2</sup> vastly reduced the simulation time of the FE<sup>2</sup> method in Example 1 to 2% w.r.t. the HF method when only the online time is considered and to 5% if the whole simulation effort is taken into account.

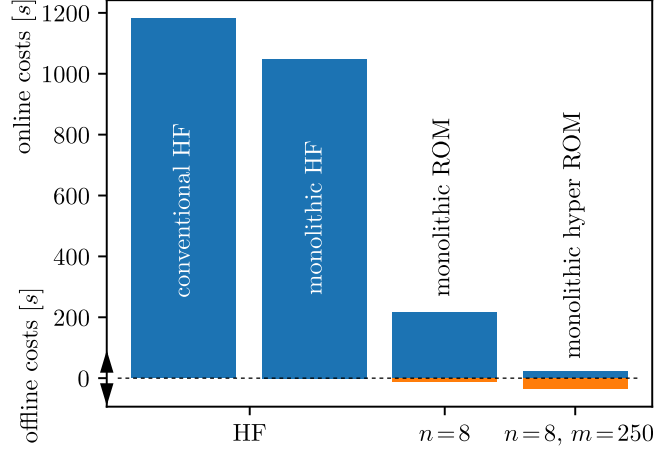


Figure 11: online/offline Simulation times Example 1

	conventional HF	monolithic HF	ROM	hyper ROM
DOFs	16 385 400 (100%)		14 400 (<1%)	
IPs	12 209 400 (100%)			450 000 (4%)
online time	1 181 s (100%)	1 048 s (89%)	215 s (18%)	23 s (2%)
offline ROM	-		12 s	
offline hyper	-		21 s	

Table 1: Simulation effort Example 1: ROM offline time includes simulation of the beam with a replacement model, training RVE-FE simulations and SVD on  $\underline{x}_u$ , hyper offline time includes training ROM-RVE-FE simulations, SVD on  $\underline{x}_f$  and ECM selection

### 5.3. Example 2: ceramic flow through filter

For the second example a flow through foam filter is considered as depicted in Figure 12 (a). Such filters are used in casting processes to filter out unwanted constituents from the metal melt. The flow through melt acts like a volume force from a mechanical viewpoint. Details can be found in [26]. On the macro scale an axis symmetric model with linear, fully integrated Abaqus elements CAX4 at large deformations are used, whereby the contact between filter and coating is described by Coulomb friction with  $\mu = 0.3$ . The loading is raised linearly in the first first second and then held constant for two hours as can be seen in Figure 12 (b). The RVE and its mesh is taken from [26] (parameters:  $k = 0.75$ ,  $\varrho_{\text{rel}} = 0.20$ ). The material behavior is represented through a hypo elastic creep model in strain hardening form. The Jaumann rate of the stress  $\overset{\nabla}{\underline{\sigma}}$  reads

$$\overset{\nabla}{\underline{\sigma}} = 3K \cdot \text{sph}(\underline{d}) + 2\mu \cdot \left[ \text{dev}(\underline{d}) - \frac{3}{2} \frac{\text{dev}(\underline{\sigma})}{\sigma_{\text{eq}}} \cdot \underline{\varepsilon}_{\text{eq}}^{\text{cr}} \right], \quad \underline{\varepsilon}_{\text{eq}}^{\text{cr}} = \left[ \frac{\sigma_{\text{eq}}}{A} \right]^{\frac{n}{m+1}} \left[ (m+1) \varepsilon_{\text{eq}}^{\text{cr}} \right]^{\frac{m}{m+1}}, \quad \sigma_{\text{eq}} = \sqrt{3J_2}. \quad (26)$$

The equations are discretized by means of the Euler implicit scheme. Globally the Update Lagrange method is applied by using the configuration of the last timestep as reference frame and evaluating the rate of deformation tensor  $\underline{d}$  through the midpoint rule after Hughes and Winget [19].

At first a simulation of the macroscopic problem with “effective” properties using the constitutive law (26) is conducted, whereby the initial stiffness is assumed to be orthotropic and condensed out of the RVE-FE model

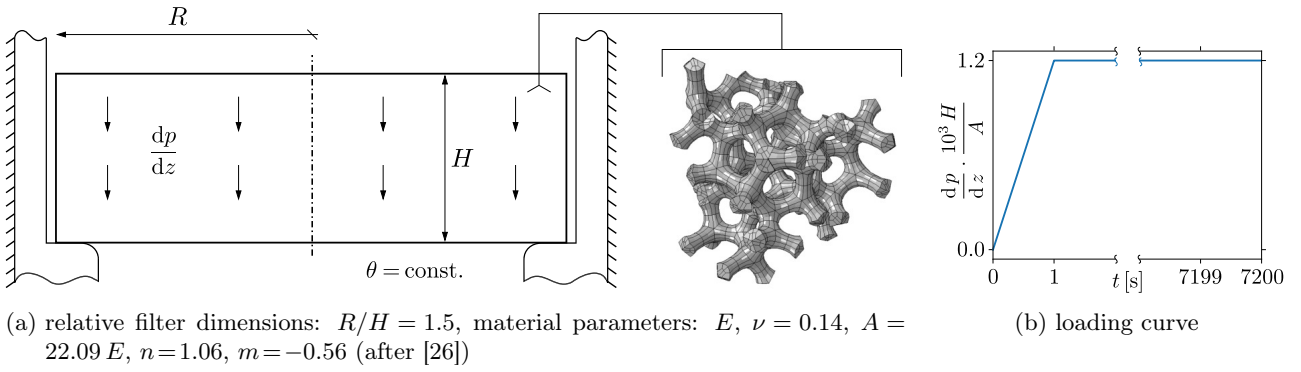


Figure 12: Example 2: Ceramic flow through foam filter at high temperatures, examination of creep behavior for 2h of metal flowing

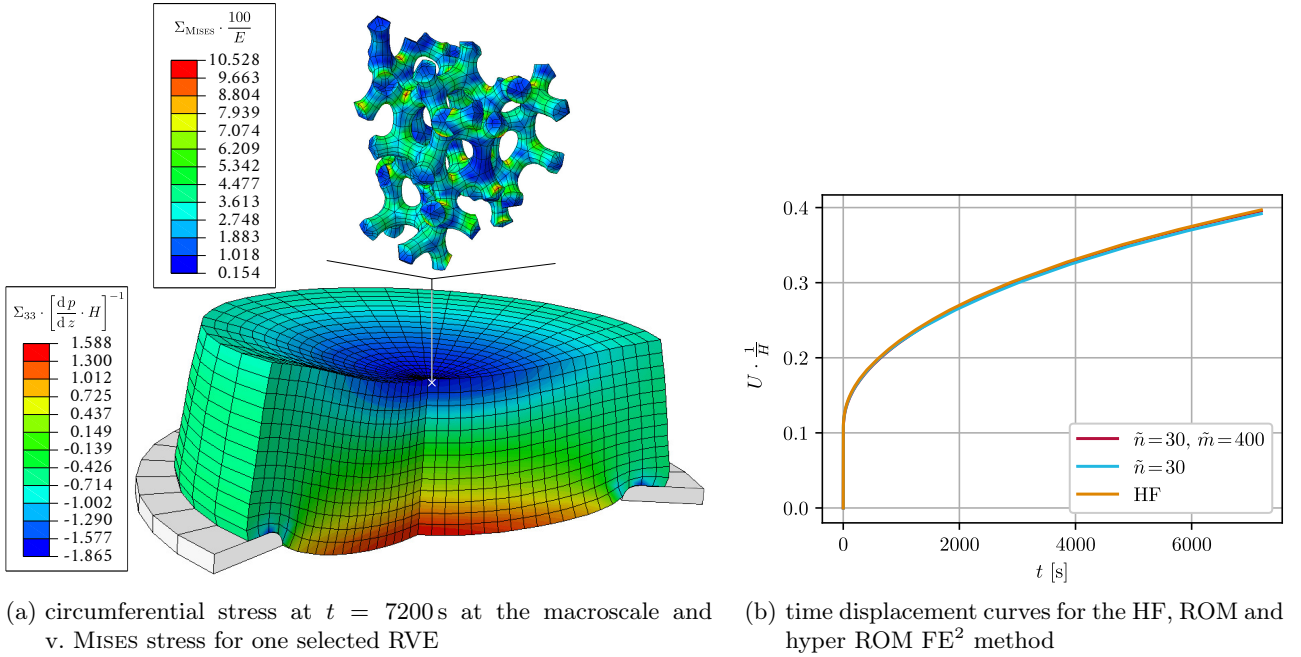


Figure 13: Final simulation result for creeping of a ceramic flow through foam filter

and  $A$  is fitted using a simple tension test. The stress state at  $t = 7200\text{s}$  is clustered. Afterwards the training is set up using the stress clusters with its loading paths following the same pattern as the actual global loading as shown in Figure 12 (b). From the resulting training data  $\tilde{n} = 30$  modes are extracted. Then the training is repeated using the ROM method and  $\tilde{m} = 500$  hyper integration points are extracted using the ECM algorithm.

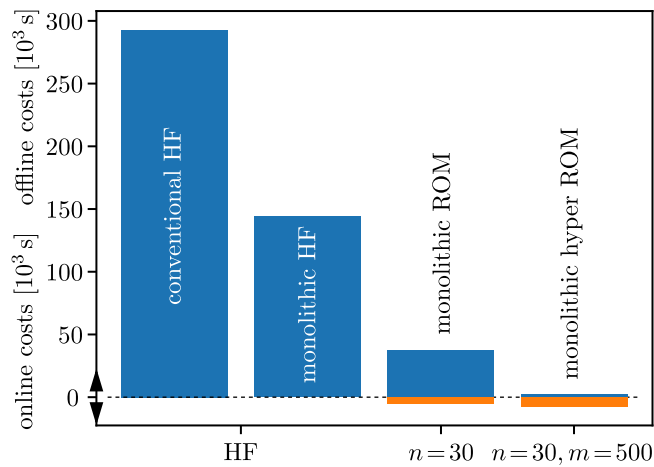


Figure 14: Simulation times Example 2

Figure 13 shows the simulation results, whereat on the left the macroscopic circumferential stress can be seen and the von MISES stress for a selected RVE and on the right the macroscopic  $U$ - $t$ -curve for all simulation methods. All three curves show a good agreement, also in terms of the local measures. The simulation effort is shown in Figure 14 and Table 1. The simulation effort in terms of the online time amounts to 13% for the ROM and below 1% in the hyper ROM case. When additionally the offline costs are considered, the total simulation costs are 15% and 3% of the ROM resp. hyper ROM method compared to the conventional HF model.

	conventional HF	monolithic HF	ROM	hyper ROM
DOFs	51 858 560 (100%)		31 200 (<1%)	
IPs	93 000 960 (100%)			520 000 (<1%)
online time	292 819 s (100%)	143 837 s (49%)	37 551 s (13%)	2 077 s (<1%)
offline ROM	-		4 959 s	
offline hyper	-			2 550 s

Table 2: Simulation effort Example 2: ROM offline time includes simulation of the filter with a replacement model, training RVE-FE simulations and SVD on  $\underline{x}_u$ , hyper offline time includes training ROM-RVE-FE simulations, SVD on  $\underline{x}_f$  and ECM selection

## 6. Conclusion

The conventional formulation of the  $FE^2$  method represents a very flexible tool for multiscale simulations. The enormous costs are a hindrance for its application in the engineering environment. The hyper ROM method seems to be a promising approximation technique, because it still solves the original PDE, while the results lie in reduced spaces, since a lot of correlation can be observed in the full model. The main advantage therefore is that a lot of the flexibility of the unreduced  $FE^2$  method is preserved, while the computational costs are reduced drastically. In comparison to common hybrid Neural Network approaches, the online costs will be higher, however less training effort is needed and the method promises more flexibility.

A formulation based on the work of Hernández et al. [16] applicable at large deformations has been presented and combined with a monolithic solution scheme. The necessary amount of training data was vastly reduced by clustering loading paths from the structure of interest. Numerical examples prove the applicability for practical problems and a speedup factor of up to 140 regarding the online simulation time was observed in comparison to the conventional  $FE^2$  scheme. It was also empirically shown, that the clustered training strategy not only reduces the training effort, but lowers the number of modes necessary in the online phase.

In comparing the obtained efficiency improvement measured by the speedupfactor w.r.t. the conventional  $FE^2$  method with those observed in literature, at least four factors should be taken into account. Firstly in some publications the speedupfactor relates to RVE simulations, not actual multiscale simulations. Secondly the complexity of the material formulations differs considerably among the papers. Thirdly the publications use different accuracy requirements and fourthly the redundancy of the RVEs' geometries and the mesh densities must be assessed. The last factor is the most important one, because the main effect of the ROM method is to "filter out" redundancies, of which more is expected, if the geometry repeats in some way and the mesh density is very high. For example in the works of Raschi et al. [37] the speedup of a composite RVE with different fibre stackings was in a range from  $\approx 10$  to  $\approx 10^4$  depending on the redundancy in the geometry. Exemplary Rocha et al. [38] obtain a speedupfactor of 270 and Caicedo et al. [3] give a speedupfactor of 170-302, depending on the accuracy requirement. Other papers will come to comparable results, but the actual values strongly depend on the aforementioned factors.

Finally we conclude, that the combination of the presented methods in this paper lie in terms of efficiency in the order of those observed in literature. However in many publications the offline effort is not quantified properly and the simulations settings differ substantially and are therefore difficult to be compared. Further research will show, which methods should be combined in the most effective way, to get robust and reliable simulation results in the multiscale context, while assuring low numerical costs and preserving most of the flexibility of the conventional  $FE^2$  method.

## Acknowledgment

The author NL gratefully acknowledges the financial support by the Deutsche Forschungsgemeinschaft within project 397252409 ‘‘Compute Cluster zur Zentralisierung der Rechenbedarfe’’.

## A. Derivation of the algorithmically consistent tangent

To get the algorithmic consistent tangent with respect to the cauchy stress and the rate of deformation as needed by FE codes using the Update Lagrange formulation, approximations must be made, because at the material point level usually the relation  $\underline{\dot{U}}^{n+1} = \underline{\dot{U}}^{n+1}(\underline{D}^{n+1})$  is not known since  $\underline{D}^{n+1}$  is computed using an approximation (usually midpoint configuration after Hughes and Winget) which is only known at the element level. The quality of the approximation must be confirmed empirically. The tangent can be found by applying the product rule

$$\frac{d\underline{\Sigma}}{d\underline{D}} = \frac{d\underline{\Sigma}}{d\underline{\Sigma}^B} : \frac{d\underline{\Sigma}^B}{d\underline{\dot{U}}} : \frac{d\underline{\dot{U}}}{d\underline{D}} = \frac{d\underline{\Sigma}}{d\underline{\Sigma}^B} : \underline{\underline{C}}^B : \frac{d\underline{\dot{U}}}{d\underline{D}}, \quad \text{with} \quad \underline{\underline{C}}^B = \frac{d\underline{\Sigma}^B}{d\underline{\dot{U}}}. \quad (27)$$

Thereby  $\frac{d\underline{\Sigma}}{d\underline{\Sigma}^B}$  is computed from equation (16) as

$$\frac{d\underline{\Sigma}}{d\underline{\Sigma}^B} = \frac{2}{J} [R_{ik} F_{lj}^{-1} + F_{ki}^{-1} R_{jl}]^{-1} \underline{e}_i \otimes \underline{e}_j \otimes \underline{e}_k \otimes \underline{e}_l \quad (28)$$

From the RVE’s FE system matrix  $\underline{\underline{C}}^B$  can be condensed out as shown in equation (19). The last term of equation (27) can only be approximated, whereby the following approximation, which assumes a constant rotation over the time step ( $\underline{\dot{R}} \approx \underline{0}$ ) and thereby corresponding to the idea of the Update Lagrange Scheme, yields good results

$$\underline{\dot{U}} = \underline{R}^T \cdot [\underline{D} + \underline{W}] \cdot \underline{F} - \underline{R}^T \cdot \underline{\dot{R}} \cdot \underline{U}, \quad \frac{d\underline{\dot{U}}}{d\underline{D}} \approx R_{ki} F_{lj} \underline{e}_i \otimes \underline{e}_j \otimes \underline{e}_k \otimes \underline{e}_l. \quad (29)$$

Equations (27)-(29) together yield

$$\frac{d\underline{\Sigma}}{d\underline{D}} \approx \frac{2}{J} [R_{im} F_{nj}^{-1} + F_{mi}^{-1} R_{jn}]^{-1} C_{mnop}^B R_{ko} F_{lp} \underline{e}_i \otimes \underline{e}_j \otimes \underline{e}_k \otimes \underline{e}_l. \quad (30)$$

## References

- [1] An, S., Kim, T., James, D., 2009. Optimizing Cubature for Efficient Integration of Subspace Deformations. *ACM transactions on graphics* 27, 165. doi:10.1145/1409060.1409118.
- [2] Bebendorf, M., Maday, Y., Stamm, B., 2014. Comparison of Some Reduced Representation Approximations, in: Quarteroni, A., Rozza, G. (Eds.), *Reduced Order Methods for Modeling and Computational Reduction*. Springer International Publishing, chapter 3, pp. 67–100. doi:10.1007/978-3-319-02090-7\_3.
- [3] Caicedo, M., Mroginski, J.L., Toro, S., Raschi, M., Huespe, A., Oliver, J., 2019. High Performance Reduced Order Modeling Techniques Based on Optimal Energy Quadrature: Application to Geometrically Non-linear Multiscale Inelastic Material Modeling. *Archives of Computational Methods in Engineering* 26. doi:10.1007/s11831-018-9258-3.
- [4] Eidel, B., Fischer, A., 2018. The heterogeneous multiscale finite element method for the homogenization of linear elastic solids and a comparison with the FE<sup>2</sup> method. *Computer Methods in Applied Mechanics and Engineering* 329, 332–368. doi:10.1016/j.cma.2017.10.001.
- [5] Eidel, B., Fischer, A., Ajinkya, G., 2019. A Nonlinear Finite Element Heterogeneous Multiscale Method for the Homogenization of Hyperelastic Solids and a Novel Staggered Two-Scale Solution Algorithm doi:10.48550/arxiv.1908.08292.
- [6] Feyel, F., 1999. Multiscale FE<sup>2</sup> elastoviscoplastic analysis of composite structures. *Computational Materials Science* 16, 344–354. doi:10.1016/S0927-0256(99)00077-4.

- [7] Fish, J., Wagner, G., Keten, S., 2021. Mesoscopic and multiscale modelling in materials. *Nature Materials* 20, 774–786. doi:10.1038/s41563-020-00913-0.
- [8] Fritzen, F., Fernández, M., Larsson, F., 2019. On-the-Fly Adaptivity for Nonlinear Twoscale Simulations Using Artificial Neural Networks and Reduced Order Modeling. *Frontiers in Materials* 6. doi:10.3389/fmats.2019.00075.
- [9] Fritzen, F., Leuschner, M., 2013. Reduced basis hybrid computational homogenization based on a mixed incremental formulation. *Computer Methods in Applied Mechanics and Engineering* 260, 143–154. doi:10.1016/j.cma.2013.03.007.
- [10] Gajek, S., Schneider, M., Böhlke, T., 2020. On the micromechanics of deep material networks. *Journal of the Mechanics and Physics of Solids* 142, 103984. doi:10.1016/j.jmps.2020.103984.
- [11] Geers, M., Kouznetsova, V., Brekelmans, W., 2010. Multi-scale computational homogenization: Trends and challenges. *Journal of Computational and Applied Mathematics* 234, 2175–2182. doi:10.1016/j.cam.2009.08.077. fourth International Conference on Advanced COmputational Methods in ENgineering (ACOMEN 2008).
- [12] Geers, M.G.D., Kouznetsova, V.G., Matouš, K., Yvonnet, J., 2017. Homogenization Methods and Multi-scale Modeling: Nonlinear Problems. American Cancer Society. pp. 1–34. doi:10.1002/9781119176817.ecm2107.
- [13] Han, J., Kamber, M., Pei, J., 2012. 10 – Cluster Analysis: Basic Concepts and Methods, in: Han, J., Kamber, M., Pei, J. (Eds.), *Data Mining (Third Edition)*. Morgan Kaufmann. The Morgan Kaufmann Series in Data Management Systems, pp. 443–495. doi:10.1016/B978-0-12-381479-1.00010-1.
- [14] Hernandez, J., 2020. A multiscale method for periodic structures using domain decomposition and ECM-hyperreduction. *Computer Methods in Applied Mechanics and Engineering* 368, 113192. doi:10.1016/j.cma.2020.113192.
- [15] Hernandez, J., Caicedo-Silva, M., Ferrer Ferre, A., 2016. Dimensional hyper-reduction of nonlinear finite element models via empirical cubature. *Computer Methods in Applied Mechanics and Engineering* 313. doi:10.1016/j.cma.2016.10.022.
- [16] Hernández, J., Oliver, J., Huespe, A., Caicedo, M., Cante, J., 2014. High-performance model reduction techniques in computational multiscale homogenization. *Computer Methods in Applied Mechanics and Engineering* 276, 149–189. doi:10.1016/j.cma.2014.03.011.
- [17] Hill, R., 1972. On constitutive macro-variables for heterogeneous solids at finite strain. *Proceedings of the Royal Society of London. A. Mathematical and Physical Sciences* 326, 131–147. doi:10.1098/rspa.1972.0001.
- [18] Hirsekorn, S., 1990. Elastic properties of polycrystals: a review. *Textures and Microstructures* 12(1-3), 1–14.
- [19] Hughes, T.J.R., Winget, J., 1980. Finite rotation effects in numerical integration of rate constitutive equations arising in large-deformation analysis. *International Journal for Numerical Methods in Engineering* 15, 1862–1867. doi:10.1002/nme.1620151210.
- [20] Jang, D., Fazily, P., Yoon, J., 2020. Machine Learning-Based Constitutive Model for J2- Plasticity. *International Journal of Plasticity* 138, 102919. doi:10.1016/j.ijplas.2020.102919.
- [21] Jänicke, R., Larsson, F., Runesson, K., Steeb, H., 2016. Numerical identification of a viscoelastic substitute model for heterogeneous poroelastic media by a reduced order homogenization approach. *Computer Methods in Applied Mechanics and Engineering* 298, 108–120. doi:10.1016/j.cma.2015.09.024.
- [22] Kalina, K.A., Linden, L., Brummund, J., Kästner, M., 2022. FEANN – An efficient data-driven multiscale approach based on physics-constrained neural networks and automated data mining. doi:10.48550/arXiv.2207.01045.
- [23] Kanouté, P., Boso, D., Chaboche, J., Schrefler, B.A., 2009. Multiscale Methods for Composites: A Review. *Archives of Computational Methods in Engineering* 16, 31–75. doi:10.1007/s11831-008-9028-8.
- [24] Kochmann, J., Brepols, T., Wulfinghoff, S., Svendsen, B., Reese, S., 2018. On the computation of the exact overall consistent tangent moduli for non-linear finite strain homogenization problems using six finite perturbations. conference paper ECCM 6 doi:10.13140/RG.2.2.32906.36809.

- [25] Lange, N., Hütter, G., Kiefer, B., 2021. An efficient monolithic solution scheme for FE<sup>2</sup> problems. *Computer Methods in Applied Mechanics and Engineering* 382, 113886. doi:10.1016/j.cma.2021.113886.
- [26] Lange, N., Hütter, G., Kiefer, B., 2022. Influence of the Foam Morphology on the Mechanical Behavior of Flow-Through Foam Filters During Filtration Processes. *Advanced Engineering Materials* 24 - No. 2, 2100784. doi:10.1002/adem.202100784.
- [27] Liu, X., Tian, S., Tao, F., Yu, W., 2021. A review of artificial neural networks in the constitutive modeling of composite materials. *Composites Part B: Engineering* 224, 109152. doi:10.1016/j.compositesb.2021.109152.
- [28] Liu, Z., Wu, C., Koishi, M., 2019. A deep material network for multiscale topology learning and accelerated nonlinear modeling of heterogeneous materials. *Computer Methods in Applied Mechanics and Engineering* 345, 1138–1168. URL: <https://www.sciencedirect.com/science/article/pii/S0045782518304729>, doi:10.1016/j.cma.2018.09.020.
- [29] Lloyd, S., 1982. Least squares quantization in PCM. *IEEE Transactions on Information Theory* 28, 129–137. doi:10.1109/TIT.1982.1056489.
- [30] Logarzo, H.J., Capuano, G., Rimoli, J.J., 2021. Smart constitutive laws: Inelastic homogenization through machine learning. *Computer Methods in Applied Mechanics and Engineering* 373, 113482. doi:10.1016/j.cma.2020.113482.
- [31] Malik, A., Abendroth, M., Hütter, G., Kiefer, B., 2022. A Hybrid Approach Employing Neural Networks to Simulate the Elasto-Plastic Deformation Behavior of 3D-Foam Structures. *Advanced Engineering Materials* 24, 2100641. doi:10.1002/adem.202100641.
- [32] Matouš, K., Geers, M.G., Kouznetsova, V.G., Gillman, A., 2017. A review of predictive nonlinear theories for multiscale modeling of heterogeneous materials. *Journal of Computational Physics* 330, 192–220. doi:10.1016/j.jcp.2016.10.070.
- [33] Miehe, C., Koch, A., 2002. Computational micro-to-macro transitions of discretized microstructures undergoing small strains. *Archive of Applied Mechanics* 72, 300–317.
- [34] Mori, T., Tanaka, K., 1973. Average stress in matrix and average elastic energy of materials with misfitting inclusions. *Acta Metallurgica* 21, 571–574. doi:10.1016/0001-6160(73)90064-3.
- [35] Qu, T., Di, S., Feng, Y., Wang, M., Zhao, T., 2021. Towards data-driven constitutive modelling for granular materials via micromechanics-informed deep learning. *International Journal of Plasticity* , 103046doi:10.1016/j.ijplas.2021.103046.
- [36] Raju, K., Tay, T.E., Tan, V.B.C., 2021. A review of the FE<sup>2</sup> method for composites. *Multiscale and Multidisciplinary Modeling, Experiments and Design* 4, 1–24. doi:10.1007/s41939-020-00087-x.
- [37] Raschi, M., Lloberas-Valls, O., Huespe, A., Oliver, J., 2021. High performance reduction technique for multiscale finite element modeling (HPR-FE<sup>2</sup>): Towards industrial multiscale FE software. *Computer Methods in Applied Mechanics and Engineering* 375, 113580. doi:10.1016/j.cma.2020.113580.
- [38] Rocha, I., Kerfriden, P., Van der Meer, F., 2020. Micromechanics-based surrogate models for the response of composites: A critical comparison between a classical mesoscale constitutive model, hyper-reduction and neural networks. *European Journal of Mechanics - A/Solids* 82, 103995. doi:10.1016/j.euromechsol.2020.103995.
- [39] Rocha, I., Van der Meer, F., Sluys, L., 2018. Efficient micromechanical analysis of fiber-reinforced composites subjected to cyclic loading through time homogenization and reduced-order modeling. *Computer Methods in Applied Mechanics and Engineering* 345. doi:10.1016/j.cma.2018.11.014.
- [40] Rocha, I., Van der Meer, F., Sluys, L., 2019. An adaptive domain-based POD/ECM hyper-reduced modeling framework without offline training. *Computer Methods in Applied Mechanics and Engineering* 358. doi:10.1016/j.cma.2019.112650.
- [41] Schröder, J., 2014. A numerical two-scale homogenization scheme: the FE<sup>2</sup>-method, in: Schröder, J., Hackl, K. (Eds.), *Plasticity and Beyond: Microstructures, Crystal-Plasticity and Phase Transitions*. Springer, Vienna, pp. 1–64.
- [42] Settgast, C., Hütter, G., Kuna, M., Abendroth, M., 2020. A hybrid approach to simulate the homogenized irreversible elastic–plastic deformations and damage of foams by neural networks. *International Journal of Plasticity* 126, 102624. doi:10.1016/j.ijplas.2019.11.003.

- [43] Sharba, S., Herb, J., Fritzen, F., 2023. Reduced order homogenization of thermoelastic materials with strong temperature dependence and comparison to a machine-learned model. *Archive of Applied Mechanics* 93, 2855–2876. doi:10.1007/s00419-023-02411-6.
- [44] Soldner, D., Brands, B., Zabihyan, R., Steinmann, P., 2017. A numerical study of different projection-based model reduction techniques applied to computational homogenisation. *Computational Mechanics* 60. doi:10.1007/s00466-017-1428-x.
- [45] Soldner, D., Brands, B., Zabihyan, R., Steinmann, P., Mergheim, J., 2016. Computational Homogenisation using Reduced-Order Modelling applied to Hyperelasticity. *PAMM* 16, 551–552. doi:10.1002/pamm.201610264.
- [46] van Tuijl, R., Remmers, J., Geers, M., 2018. Integration efficiency for model reduction in micro-mechanical analyses. *Computational Mechanics* 62. doi:10.1007/s00466-017-1490-4.
- [47] Waimann, J., Gierden, C., Schmidt, A., Svendsen, B., Reese, S., 2022. Reduced FFT-Based Simulation of a Mechanically Loaded Clustered Microstructure Using an Adaptive Set of Fourier Modes. *Key Engineering Materials* 926, 2285–2292. doi:10.4028/p-9cr29c.